Hindawi
International Journal of Antennas and Propagation
Volume 2023, Article ID 5551000, 9 pages
https://doi.org/10.1155/2023/5551000

Research Article

A Computationally Efficient Estimator for the Target Angle, Delay, and Doppler Parameters in Passive Radar

Jing Yang,[1] **Chengcheng Liu**,[1] **Jie Huang**,[1] **Dapeng Liu**,[2] **Ting Ding**,[3] **Jiandong Zhu**,[3] **and Xia Li**[1]

[1]*National Digital Switching System Engineering and Technological Research Center, Zhengzhou 450001, China*
[2]*China Aerospace Science and Technology Corporation the 9th Academy, Beijing 100094, China*
[3]*Henan High-Speed Railway Operation and Maintenance Engineering Research Center, Zhengzhou 450018, China*

Correspondence should be addressed to Chengcheng Liu; luckylcc079@126.com

Received 5 December 2022; Revised 21 March 2023; Accepted 23 June 2023; Published 18 July 2023

Academic Editor: Stefano Selleri

The azimuth, elevation, time delay (TD), and Doppler shift (DS) of the target echo signal are important parameters for target localization in passive radar. In this paper, for the problem of joint estimation of target azimuth, elevation, TD, and DS parameters in passive radar, a computationally efficient estimator is proposed based on segmented coherent integration and uniform circular array (UCA) interferometer direction finding. First, according to the parameters of the target motion and illuminators of opportunity, the reference and surveillance signals are divided into segments, with fast time within a segment and slow time across the segments; then, matching filtering along the fast time and fast Fourier transform (FFT) along the slow time are performed to accumulate the target echo energy to the same delay-Doppler cell; finally, the UCA interferometer two-dimensional direction finding is performed at the delay-Doppler cell where the target echo is located, to achieve the target azimuth and elevation estimate. Simulation results demonstrate that the proposed algorithm has low computational complexity, high real-time processing capability, and can achieve efficient and real-time estimation of the azimuth, elevation, TD, and DS parameters of weak target echoes in passive radar.

1. Introduction

Passive radar (PR) systems employ existing emitters in the surrounding environment as illuminators of opportunity (IOOs) for target detection and localization [1, 2]. IOOs employed by PR include television broadcasts, audio broadcasts, mobile communications, and noncooperative radars [3, 4]. Since PR does not require any expensive dedicated transmitters in terms of hardware, it can be used for low-cost covert detection of targets and is immune to directional electronic interference [5]. PR systems have been extensively studied in recent decades due to these unique advantages over active radars.

However, unlike active radar, due to the noncooperative nature of the IOO, a PR system typically deploys two receiving channels, a reference channel for receiving the direct path signal from the IOO and a surveillance channel for receiving and detecting the IOO signal reflected back from the target [6]. Due to the reflection/scattering from the target, the target echo received by the surveillance channel has a time delay (TD) with respect to the reference signal. By estimating the TD of the target echo with respect to the reference signal, information on the target range can be determined. Due to the influence of the target motion, there is a Doppler shift (DS) between the target echo and the reference signal. By determining the DS, the velocity information of the target can be inferred. In addition, when an antenna array is employed for the surveillance channel, the angle of arrival (AOA) of the target echo can also be obtained, thus providing additional observations for target localization.

Currently, a lot of research has been conducted in academia on the target localization using AOA, TD, and DS measurements in PR, and a series of algorithms have been

developed, all of which rely on the AOA, TD, and DS parameters extracted from the target echo [7–10]. However, the problem of estimating the AOA, TD, and DS parameters in PR is still relatively little studied in the open literature. In PR systems, the target echo signal is usually very weak and drowned in the noise and clutter background, making it difficult to achieve the direct target direction finding. In order to achieve the joint estimation of AOA, TD, and DS parameters in PR, references [11, 12] first perform the delay-Doppler 2-dimensional correlation between the target echo and the reference signal using the cross-ambiguity function (CAF) to improve the signal-to-noise ratio (SNR) of the target echo, and then interferometer direction finding is performed on the delay-Doppler cell where the target is located to obtain the AOA. However, the algorithms in [11, 12] have two significant problems: first, the computational complexity of the CAF is very high and difficult to implement in real time; although some fast implementation methods [13–15] can reduce the computational cost to a certain extent, the implementation process is still complex and not applicable for some low computing power PR platforms; second, the algorithms in [11, 12] can only achieve the estimation of the target azimuth angle in 2-dimensional plane and cannot estimate the target elevation, so it is not applicable to the current target localization scenarios in 3D space. Some coherent integration methods and DOA estimation methods have been proposed for the estimation of AOA, TD, and DS parameters in active radars [16, 17]. However, these algorithms [16, 17] cannot be applied to PR due to the noncooperative nature of the IOOs.

In this paper, we address designing a computationally efficient estimator for target TD, DS, azimuth, and elevation parameters in a PR system with low computing capacity. The uniform circular array (UCA) has been often used and studied in the field of PR due to its capacities of omnidirectional coverage, two-dimensional angular resolution in azimuth and elevation, and the same resolution along a 360 degree azimuth direction. In this paper, we consider a PR using three-element UCA. A computationally efficient estimator based on segmented coherent integration and UCA interferometer direction finding is proposed for the joint estimation of the target azimuth, elevation, TD, and DS parameter.

The main advantages and innovations of our proposed algorithm, which are supported by various simulation scenarios in Section 5, include the following:

(1) The use of UCA to receive the target echo signal and use the azimuth-elevation-delay-Doppler parameters of the echo signal for target localization has received great attention in the field of passive radar. However, to our knowledge, there is a lack of specific algorithm for the computationally efficient estimation of azimuth-elevation-delay-Doppler parameters in this scenario. For this reason, this paper innovatively gives a specific algorithm for this problem.

(2) The proposed algorithm innovatively introduces segmentation processing to the joint estimation problem of azimuth-elevation-delay-Doppler parameters for passive radar, and by using signal segmentation and efficient FFT, IFFT operations, and the proposed algorithm can greatly reduce the computational complexity without causing any loss of parameter estimation performance.

2. Signal Model

We consider a PR system as shown in Figure 1. The IOO emits electromagnetic signal from its transmitting antenna (Tx), and when this signal hits a target, some of the signal energy is reflected back to the receiving antenna (Rx) of the PR system. The PR system uses a series of signal processing processes to extract parameters such as TD, DS, AOA, and other target characteristics from the received signal to detect, locate, and identify the target.

We use a directional antenna at the receiving station Rx, pointed exclusively at the IOO Tx, as a reference antenna to receive the direct path signal from the IOO, and a UCA with $N_{\text{em}} = 3$ elements as a surveillance antenna to collect the target echo signal. Assuming that Tx transmits a complex baseband signal of $s(t)$ with a carrier frequency of f_c, the RF signal can be modelled as follows:

$$u(t) = s(t)e^{j2\pi f_c t}. \tag{1}$$

Since Tx is noncooperative, $s(t)$ is generally difficult to be known accurately. Due to the path difference between the target echo signal and the direct path signal, there is a TD between the reference signal and the surveillance signal. Neglecting the noises and clutters, the received signals from the reference antenna and the surveillance antenna can be expressed respectively, as follows:

$$\begin{aligned} s_{\text{r}}(t) &= b_r e^{j\phi_{\text{r}}} u\left(t - \frac{L(t)}{c}\right), \\ s_{\text{s},i}(t) &= b_{\text{s}} e^{j\phi_{\text{s}}} u\left(t - \frac{R_t(t) + R_r(t)}{c}\right) e^{j\phi_i}, \end{aligned} \tag{2}$$

where $s_{\text{r}}(t)$ is the received signal from the reference antenna; $s_{\text{s},i}(t)$, $i = 0, 1, \ldots, N_{\mathbf{em}} - 1$ is the received signal in the ith array element of the surveillance antenna, ; b_{r} and b_{s} are the unknown amplitude scaling resulting from the channel and receiver effects; ϕ_{r} and ϕ_{s} are the unknown phase shift; $L(t)$ is the distance between Tx and Rx; $R_{\text{t}}(t)$ and $R_{\text{r}}(t)$ are the distance from Tx to the target and the distance from the target to Rx, respectively; ϕ_i is the phase difference of the ith array element of the surveillance antenna with respect to the centre of the UCA; the azimuth and elevation angles of the target echo signal are assumed to be $\theta \in [-\pi, \pi]$ and $\varphi \in [0, (\pi/2)]$, respectively. By using the UCA centre as the reference origin, the direction vector of the target echo is given by

$$\xi = [\cos\varphi\cos\theta,\ \cos\varphi\sin\theta,\ \sin\varphi]^T. \tag{3}$$

The position of the ith array element is as follows:

$$\mathbf{x}_i = \left[R\cos\left(\frac{2\pi i}{N_{\text{em}}}\right), R\sin\left(\frac{2\pi i}{N_{\text{em}}}\right), 0\right]^T, \tag{4}$$

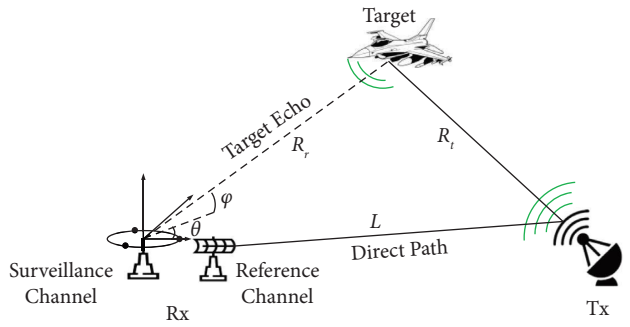

Figure 1: Signal propagation in passive radar.

where R is the radius of the UCA. In particular, to avoid phase ambiguity, the antenna array element spacing needs to satisfy

$$\frac{d}{\lambda} = \frac{2R\sin(\pi/3)}{\lambda} \leq \frac{1}{2}, \tag{5}$$

that is, the radius of the UCA needs to satisfy

$$R \leq \frac{\lambda}{2\sqrt{3}}. \tag{6}$$

The TD between the arrival of the target echo at the ith array element and its arrival at the UCA centre is as follows:

$$\begin{aligned}\tau_i &= \frac{-1}{c}\mathbf{x}_i^T\xi \\ &= -\frac{R}{c}\cos\left(\frac{2\pi i}{N_{\text{em}}}\right)\cos(\varphi)\cos(\theta) - \frac{R}{c}\sin\left(\frac{2\pi i}{N_{\text{em}}}\right)\cos(\varphi)\sin(\theta) \\ &= -\frac{R}{c}\cos(\varphi)\cos\left(\theta - \frac{2\pi i}{N_{\text{em}}}\right).\end{aligned} \tag{7}$$

Correspondingly, the phase difference between the arrival of the target echo at the ith array element and its arrival at the UCA centre is as follows:

$$\begin{aligned}\phi_i &= 2\pi f_c \tau_i \\ &= -\frac{2\pi R}{\lambda}\cos(\varphi)\cos\left(\theta - \frac{2\pi i}{N_{\text{em}}}\right).\end{aligned} \tag{8}$$

In fact, it is the difference $r(t) = R_t(t) + R_r(t) - L$ that is of interest and exploited for target localization. After performing some variable substitution and simplification, one can obtain the following:

$$\begin{aligned}s_r(t) &= u(t), \\ s_{s,i}(t) &= be^{j\phi}u\left(t - \frac{r(t)}{c}\right)e^{j\phi_i},\end{aligned} \tag{9}$$

where $b = (b_s/b_r)$ and $\phi = \phi_s - \phi_r$. The information about the target position is contained in $r(t)$, which can be expanded at $t = 0$ using the Taylor series as follows:

$$r(t) = c\tau + vt + , \ldots, \tag{10}$$

where τ represents the initial time delay of the target echo at $t = 0$ and v represents the Doppler velocity.

After down-converting the signal, the received signal can be written as follows:

$$\begin{aligned}s_r(t) &= s(t), \\ s_{s,i}(t) &= be^{j\phi}s\left(t - \frac{r(t)}{c}\right)e^{-j2\pi f_c(r(t)/c)}e^{j\phi_i}.\end{aligned} \tag{11}$$

3. Signal Segmentation

In passive radar, CAF is usually performed to obtain cumulative gain and improve the SNR of the target echo. However, the high computational complexity of the CAF makes it difficult to apply on low arithmetic platforms. For this reason, we artificially construct equivalent pulse signals by dividing the received reference and surveillance signals into segments and then perform coherent integration to accumulate the target echo energy to the same delay-Doppler cell. The specific segmentation method is illustrated in Figure 2.

First, based on the maximum Doppler velocity of the potential target, the equivalent pulse repetition frequency (PRF) is determined as follows:

$$\text{PRF} = \frac{2v_{\max}}{\lambda}, \tag{12}$$

where $v_{\max}$ is the maximum Doppler velocity of the potential target and λ is the signal wavelength. Based on the equivalent PRF, the number of signal segments can be determined as follows:

$$M = T \cdot \text{PRF}, \tag{13}$$

where T is the signal accumulation time. The reference signal and the surveillance signal are segmented according to the number of segments determined previously, with the effective length of each segment being

$$N_{\text{eff}} = \frac{Tf_s}{M}, \tag{14}$$

where f_s is the sampling frequency. For the surveillance signal, to solve the conflicting relationship between the equivalent PRF and the equivalent pulse length, the surveillance signal batches are partially overlapped by extending each segment by N_τ samples, where

$$N_\tau = \tau_{\max} f_s, \tag{15}$$

with $\tau_{\max}$ being the maximum time delay of a potential target. This means that the length of each segment of the surveillance signal after overlapping is $N = N_{\text{eff}} + N_\tau$. For the reference signal, the length of each segment is kept the same as the surveillance signal by padding N_τ zeros at the end. By overlapping the segments, each segment has a sufficiently large equivalent pulse length to avoid distance ambiguity while ensuring that the segmented signal has

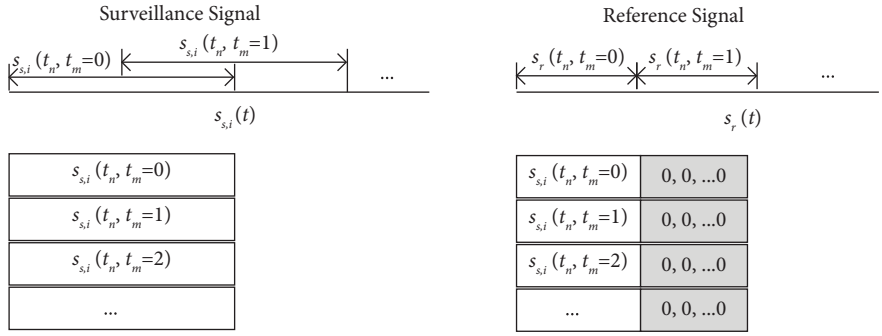

Figure 2: Schematic diagram of signal segmentation.

a large enough equivalent PRF to avoid speed ambiguity. On the other hand, the segment-overlapping of the surveillance signal and the zero-padding of the reference signal ensure that the accumulation gain of the target echo at different time delay bins remains the same.

After dividing the reference and surveillance signals into segments, the equivalent pulse signals can be constructed as follows:

$$\begin{aligned} s_{\mathrm{r}}(t_n, t_m) &= s(t_n), \\ s_{\mathrm{s},i}(t_n, t_m) &= be^{j\phi} s\left(t_n - \frac{r(t_m)}{c}\right) e^{-j2\pi f_{\mathrm{c}}(r(t_m)/c)} e^{j\phi_i}, \end{aligned} \tag{16}$$

where $t_n = (n/f_s)$ represents the fast time, $n = 0, 1, \ldots, N-1$; $t_m = (m/\mathrm{PRF})$ represents the slow time, $m = 0, 1, \ldots, M-1$.

4. TD-DS-AOA Estimation

4.1. Delay-Doppler Processing. Performing the fast Fourier transform along the fast time t_n, we get

$$\begin{aligned} S_r(f_n, t_m) &= S(f_n), \\ S_{\mathrm{s},i}(f_n, t_m) &= be^{j\phi} S(f_n) e^{-j2\pi(f_{\mathrm{c}}+f_n)(r(t_m)/c)} e^{j\phi_i}, \end{aligned} \tag{17}$$

where $S(f_n) = \mathrm{FFT}[s(t_n)]$. Multiplying $S_{\mathrm{s},i}(f_n, t_m)$ with the conjugate of $S_r(f_n, t_m)$ yields

$$\begin{aligned} Y_i(f_n, t_m) &= S_{\mathrm{s},i}(f_n, t_m) S_r^*(f_n, t_m) \\ &= be^{j\phi} |S(f_n)|^2 e^{-j2\pi(f_{\mathrm{c}}+f_n)(r(t_m)/c)} e^{j\phi_i}, \end{aligned} \tag{18}$$

where $*$ denotes the conjugate operation. Performing the inverse FFT on (18) along f_n gives

$$y_i(t_n, t_m) = be^{j\phi} p\left(t_n - \frac{r(t_m)}{c}\right) \mathrm{e}^{-j2\pi f_{\mathrm{c}}(r(t_m)/c)} e^{j\phi_i}, \tag{19}$$

where $p(t_n) = \mathrm{IFFT}(|S(f_n)|^2)$ has its peak at $t = 0$. From equation (19), it can be seen that the target envelope is distributed at $(r(t_m)/c)$. Since the baseband signal $s(t)$ is a narrowband signal, it can be generally assumed that the offset of $r(t_m)$ does not exceed the range resolution $(c/2B)$, then equation (19) can be expressed as follows:

$$y_i(t_n, t_m) = be^{j\phi} p(t_n - \tau) e^{-j2\pi f_{\mathrm{c}}(r(t_m)/c)} e^{j\phi_i}. \tag{20}$$

Performing FFT on equation (20) along the slow time t_m, we get

$$\chi_i(t_n, f_m) = ap(t_n - \tau) \sin c\left[T\left(f_m - \frac{f_{\mathrm{c}}v}{c}\right)\right] e^{j\phi_i}, \tag{21}$$

where $a = bTe^{j\phi} e^{-j2\pi f_{\mathrm{c}}\tau}$. It can be observed from equation (21) that the target echo signal energy is accumulated to the peak of $\chi_i(t_n, f_m)$ at $(t_n, f_m) = (\tau, (f_{\mathrm{c}}v/c))$. By detecting and finding the peak of $\chi_i(t_n, f_m)$, the time delay and Doppler velocity of the target can be estimated.

4.2. Angle Estimation. After the previous delay-Doppler processing, the target echo signal in the received signal of each array element of the surveillance channel has been accumulated to the delay-Doppler cell $(\tau, (f_{\mathrm{c}}v/c))$. The peak value in the delay-Doppler cell where the target locates can be extracted as follows:

$$\begin{aligned} \chi_0\left(\tau, \frac{f_{\mathrm{c}}v}{c}\right) &= ap(0) \sin \mathrm{c}(0) e^{j\phi_0}, \\ \chi_1\left(\tau, \frac{f_{\mathrm{c}}v}{c}\right) &= ap(0) \sin \mathrm{c}(0) e^{j\phi_1}, \\ \chi_2\left(\tau, \frac{f_{\mathrm{c}}v}{c}\right) &= ap(0) \sin \mathrm{c}(0) e^{j\phi_2}. \end{aligned} \tag{22}$$

Based on equation (22), the measured phase differences between the received signals of arrays 0 and 1 and arrays 0 and 2 are extracted, respectively.

$$\begin{aligned} \widehat{\phi}_{0,1} &= \mathrm{angle}\left(\frac{\chi_0}{\chi_1}\right), \\ \widehat{\phi}_{0,2} &= \mathrm{angle}\left(\frac{\chi_0}{\chi_2}\right), \end{aligned} \tag{23}$$

where angle$(\bullet)$ returns the phase angle in the interval $[-\pi, \pi]$ for a complex number.

On the other hand, by using equation (8), one can obtain the true phase difference between array elements 0 and 1 and array elements 0 and 2, respectively, as follows:

$$\begin{aligned}\phi_{0,1} &= \phi_0 - \phi_1 \\ &= -\frac{4\pi}{\lambda} R\cos(\varphi)\sin\left(\frac{\pi}{3}\right)\sin\left(\theta - \frac{\pi}{3}\right),\end{aligned} \tag{24}$$

$$\begin{aligned}\phi_{0,2} &= \phi_0 - \phi_2 \\ &= \frac{4\pi}{\lambda} R\cos(\varphi)\sin\left(\frac{\pi}{3}\right)\sin\left(\theta + \frac{\pi}{3}\right).\end{aligned} \tag{25}$$

From equations (24) and (25), it can be further deduced that

$$\begin{aligned}\phi_s &= \phi_{0,2} + \phi_{0,1} \\ &= \frac{8\pi}{\lambda} R\sin\left(\frac{\pi}{3}\right)\cos(\varphi)\cos(\theta)\sin\left(\frac{\pi}{3}\right),\end{aligned} \tag{26}$$

$$\begin{aligned}\phi_d &= \phi_{0,2} - \phi_{0,1} \\ &= \frac{8\pi}{\lambda} R\sin\left(\frac{\pi}{3}\right)\cos(\varphi)\sin(\theta)\cos\left(\frac{\pi}{3}\right).\end{aligned} \tag{27}$$

The projection of the direction vector ξ in the direction of the target echo signal onto the XOY plane of the array is expressed in the complex form as follows:

$$\begin{aligned}\mu &= \cos(\varphi)\cos(\theta) + j\cos(\varphi)\sin(\theta) \\ &= \cos(\varphi)e^{j\theta}.\end{aligned} \tag{28}$$

Combining equations (26) and (27) into equation (28), μ can be further expressed as follows:

$$\mu = \frac{\phi_s}{(8\pi/\lambda)R\sin^2(\pi/3)} + j\frac{\phi_d}{(8\pi/\lambda)R\sin(\pi/3)\cos(\pi/3)}. \tag{29}$$

From equation (28), the estimates of azimuth and elevation angles can be obtained as follows:

$$\begin{aligned}\widehat{\theta} &= \text{angle}(\widehat{\mu}), \\ \widehat{\varphi} &= \arccos(|\widehat{\mu}|),\end{aligned} \tag{30}$$

where $\widehat{\mu}$ is the estimated value of μ by substituting the measured phase differences $\widehat{\phi}_{0,1}$ and $\widehat{\phi}_{0,1}$ into equation (29); $\arccos(\cdot)$ represents the inverse cosine function. It should be noted that the radius of the UCA satisfies $R \le (\lambda/(2\sqrt{3}))$. If the radius of the UCA exceeds this limit, the phase difference between $\widehat{\phi}_{0,1}$ and $\widehat{\phi}_{0,2}$ may cause phase ambiguity, resulting in incorrect estimates of azimuth and elevation angles. In this case, in order to obtain a correct estimate of the azimuth and elevation angles, a defuzzification process is required.

5. Simulation Experiments

In this section, Monte Carlo simulation experiments are conducted to verify the performance of the proposed algorithm. The surveillance antenna is a three-element UCA with radius $R = (\lambda/(2\sqrt{3}))$. The clutter cancellation has been performed on the received signals, and they only target the echo signal and Gaussian noises existing in the surveillance channel. The IOO emits an FM signal of the following form:

$$u(t) = \exp\left(j2\pi f_c t + j2\pi K_f \text{cumsum}(m(t))\right), \tag{31}$$

where K_f is the frequency deviation of the modulated signal in hertz (Hz); $\text{cumsum}(\cdot)$ returns the cumulative sum of the elements of a vector; $m(t)$ indicates the baseband data, and here, we set it to a random sequence of integers from 0 to 15. The specific parameters of the IOO signal are listed in Table 1.

The parameters of the target are listed in Table 2.

The parameters of the PR system are taken as shown in Table 3.

The received signal is segmented according to the parameters of the source signal of opportunity irradiation and the parameters of the maximum time delay and maximum Doppler velocity of the potential target, and the segmented parameters are shown in Table 4.

The SNR of the reference signal is 30 dB and that of the target echo signal is −26 dB. It should be noted that the SNR in this paper refers to the signal-to-noise ratio of the received signal before pulse compression. As mentioned earlier, after segmenting the received signal of each array element, the reference signal is first used for match filtering of the received signal, and the result is shown in Figure 3.

From Figure 3, it can be seen that, after matched filtering, the target echo signal, which was originally submerged in noise, forms a peak in its corresponding delay cell. Then, the FFT is performed along the slow time to accumulate the echo signal energy along the slow time to the corresponding Doppler cell, and the results are shown in Figure 4.

From Figure 4, it can be seen that the echo signal energy accumulates to a peak and the peak magnitude is further enhanced. Moreover, the location of the peak matches the true TD and DS information of the target. The delay-Doppler image was detected using a two-dimensional constant false alarm rate (CFAR) detector, and the results are shown in Figure 5.

It can be seen from Figure 5 that, as expected, the target echo signal is correctly detected as the corresponding delay-Doppler cell. Extracting of the peak value at the delay-Doppler cell where the target echo is located, the direction find operation can be performed, which yields the target azimuth and elevation angles as plotted in Figure 6.

Next, we evaluate the estimation performance of the proposed algorithm under different SNR conditions. The study in [12] demonstrates that coherent integration of target echo can be achieved by CAF during delay-Doppler processing, followed by azimuth and elevation angle estimation. To highlight the advantage of the proposed algorithm, the algorithm in [12] is also involved for comparison. First, we added complex Gaussian noise with different variances to the direct path signal, which yields the received reference signal with different SNRs. The SNR of the surveillance signal was set to −20 dB and that of the reference signal was set to −30 dB~30 dB. 200 independent Monte Carlo simulations were performed for each SNR condition. The root-mean-square errors (RMSEs) of the time delay-

Table 1: Parameters of the IOO signal.

Modulation method	Carrier frequency	Bandwidth	Frequency bias constant	Bandwidth
Frequency modulation	600 MHz	1 MHz	7957.74	1 MHz

Table 2: Parameters of the target.

Parameters	Time delay	Doppler velocity	Azimuth	Pitch angle
Value	400 us	200 m/s	60°	30°

Table 3: Parameters of the passive radar system.

Sampling rate	Number of sampling points	Target maximum time delay	Target maximum Doppler velocity
1 MHz	250,000	500 us	500 m/s

Table 4: Parameters of signal segments.

PRF	M	N_{eff}	N_τ
2000	500	500	500

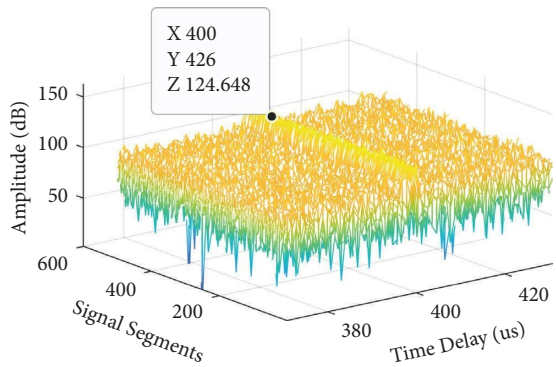

Figure 3: Results of matched filtering along fast time.

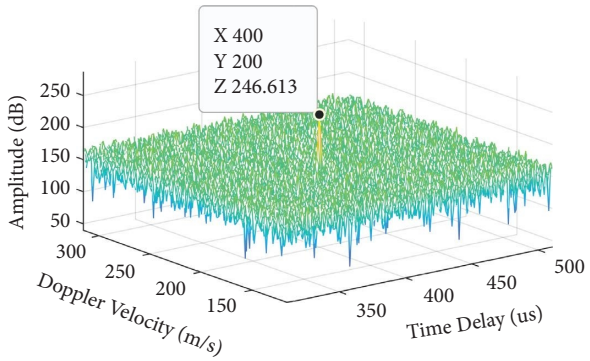

Figure 4: Delay-Doppler image.

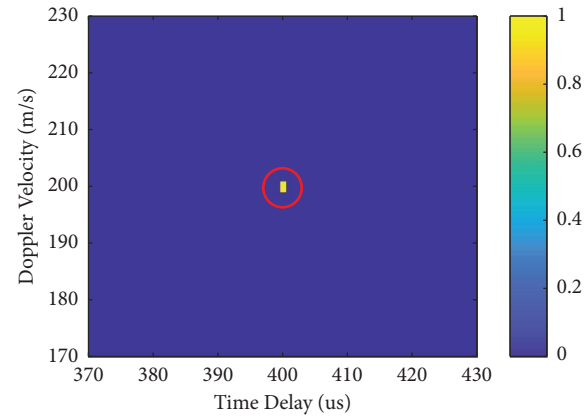

Figure 5: CFAR detection results.

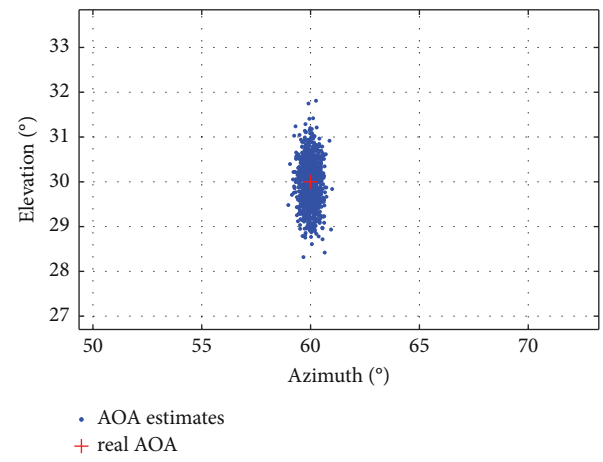

Figure 6: Scatter plot of AOA estimation results.

Doppler-azimuth and elevation estimation under the reference signal with different SNR conditions are plotted in Figure 7.

From Figure 7, it can be seen that the estimation RMSEs of the proposed algorithm for time delay, Doppler, azimuth, and elevation angles gradually decrease as the SNR of the reference signal increases. However, the SNR thresholds at which the rapid decrease in parameter estimation error occurs in (a), (b), (c), and (d) are different. In Figures 7(a) and 7(b), when the estimation RMSE of delay and Doppler decreases rapidly at around −20 dB and stabilises at a low error level after increasing to −15 dB. In Figures 7(c) and 7(d), the estimation of the azimuth and elevation angles

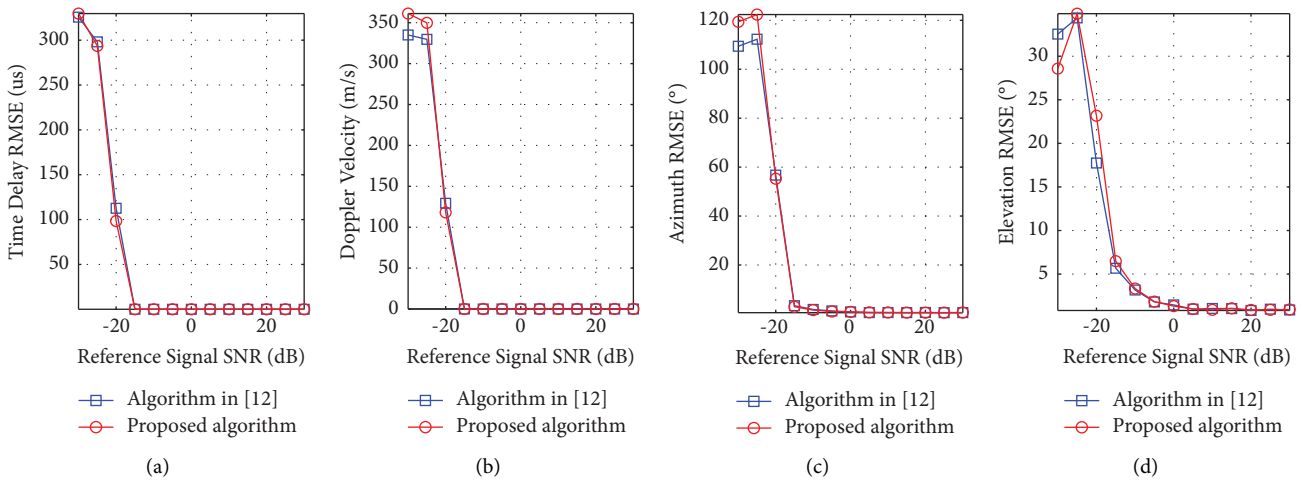

Figure 7: Estimation RMSEs under reference signals with different SNRs. (a) Time delay estimation, (b) Doppler estimation, (c) azimuth estimation, and (d) elevation estimation.

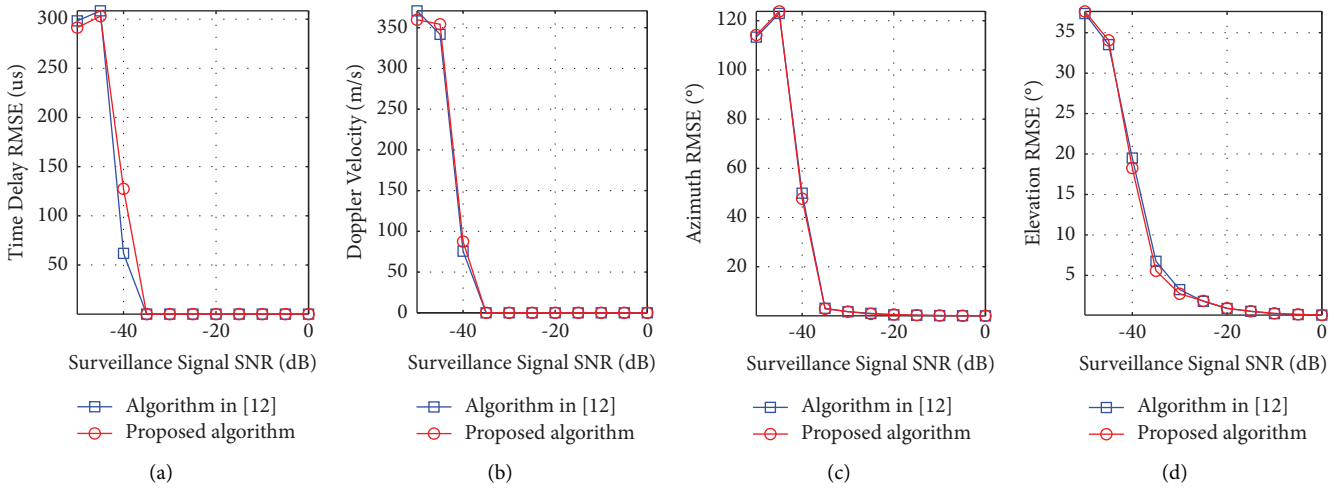

Figure 8: Estimation RMSEs under surveillance signals with different SNRs. (a) Time delay estimation, (b) Doppler estimation, (c) azimuth estimation, and (d) elevation estimation.

stabilise at low RMSE levels when the SNR of the reference signal is larger than 0 dB. This may be because the azimuth and elevation angle estimates are based on the premise that the time delay and Doppler parameters are estimated, so there may be some hysteresis between their errors. Considering that the SNR of the reference signal can easily exceed −10 dB due to the reception of the direct path signal from the IOO, it can be assumed that, under normal reception conditions, the variation of the reference signal SNR has no significant effect on the estimated performance of the time-delay-Doppler-azimuth-elevation. Moreover, compared with the algorithm in [12], the estimation RMSEs of the two algorithms are basically the same, which indicates that the proposed algorithm does not cause any loss in estimation performance while reducing the computational complexity.

Next, the SNR of the reference signal is set to 30 dB and the SNR of the surveillance signal is set to −50 dB to 0 dB. 200 independent Monte Carlo experiments are conducted for each SNR case. The RMSEs of the algorithms for the time delay-Doppler-azimuth and elevation estimates for the different SNR conditions of the surveillance signal are plotted in Figure 8.

As expected, it can be observed from Figure 8 that the proposed algorithm and the algorithm perform comparably in estimation RMSE. To be more specific, with a reference signal SNR of 30 dB, accurate estimation of the target time delay and Doppler parameters can be achieved with a surveillance signal SNR larger than −35 dB; when the surveillance signal SNR is larger than −20 dB, accurate estimation of the azimuth and elevation angles can be achieved. Considering that the target echo signal is usually very weak

Table 5: Comparison of computational complexity.

Algorithms	Theoretical computational complexity	Average running time (s)
Algorithm in [12]	$N_{\text{ele}}N_{\tau}((N_T/2)\log_2 N_T + N_T)$	82.4253
Proposed algorithm	$N_{\text{ele}}M(N\log_2 N + N) + N_{\text{ele}}N((M/2)\log_2 M)$	0.1941

in general, it is important to improve the SNR of the surveillance signal to improve the overall parameter estimation performance of the passive radar.

To demonstrate the advantage of the proposed algorithm in terms of computational complexity, we compare the theoretical computational complexity and the average running time of the two algorithms. As the computational complexity is focused on the number of complex multiplications of the delay-Doppler processing, we use this metric as the theoretical computational complexity of the algorithm. The main configuration of the computer is as follows: CPU: Intel (R) Core (TM) i7-8550U @1.80 GHz; RAM: 16 G DDR4 2666 MHz; Operating system: Windows 10; Software: MATLAB R2021b. The results of the computational complexity comparison are listed in Table 5.

In Table 5, the CAF is implemented using FFT, where $N_{\tau} = N$ is the number of time delay bins calculated and $N_T = Tf_s$ is the number of signal sampling points. Comparing the computational complexity of the two algorithms, it can be found that the proposed algorithm can reduce the computational complexity by two orders of magnitude through segmentation, which can ensure the real-time processing of the received signals.

6. Conclusion

In passive radar, the target echo is generally very weak and it is difficult to estimate the time-delay-Doppler-azimuth-elevation parameters directly. This paper proposes a computationally efficient algorithm for estimating the target time-delay-Doppler-azimuth-elevation based on segmented coherent integration and UCA interferometer direction finding. We first divide the received signals into segments according to the target motion and the IOO signal parameters and then accumulate the target echo signal energy to the same delay-Doppler cell to improve the SNR of the target echo by using matched filtering along fast time and FFT along the slow time, and finally, UCA interferometer direction finding is performed at the delay-Doppler cell of the target to obtain the target azimuth and elevation angle estimate. Simulation results verify the advantages and innovations of the proposed algorithm. Last but not the least, it should be noted that we consider a simple scenario for the sake of reducing computational complexity. However, if the computing capacity allows, the effects of range migration and Doppler migration should be considered and the long time integration algorithm can be explored to improve the parameter estimation performance.

Data Availability

Some or all data, models, or code generated or used during the study are available from the corresponding author upon request.

Conflicts of Interest

The authors declare that they have no conflicts of interest.

Acknowledgments

This work was supported by the National Natural Science Foundation of China (no. 62071490) and Natural Science Foundation of Henan (no. 222300420379).

References

[1] H. Kuschel, D. Cristallini, and K. E. Olsen, "Tutorial: passive radar tutorial," *IEEE Aerospace and Electronic Systems Magazine*, vol. 34, no. 2, pp. 2–19, 2019.

[2] P. Knott, "Design of a printed dipole antenna array for a passive radar system," *International Journal of Antennas and Propagation*, vol. 2013, Article ID 179296, 6 pages, 2013.

[3] F. Santi and D. Pastina, "A parasitic array receiver for ISAR imaging of ship targets using a coastal radar," *International Journal of Antennas and Propagation*, vol. 2016, Article ID 8485305, 11 pages, 2016.

[4] J. Palmer, S. Palumbo, A. Summers, D. Merrett, S. Searle, and S. Howard, "An overview of an illuminator of opportunity passive radar research project and its signal processing research directions," *Digital Signal Processing*, vol. 21, no. 5, pp. 593–599, 2011.

[5] M. Edrich, A. Schroeder, and F. Meyer, "Design and performance evaluation of a mature FM/DAB/DVB-T multi-illuminator passive radar system," *IET Radar, Sonar & Navigation*, vol. 8, no. 2, pp. 114–122, 2014.

[6] J. Liu, H. Li, and B. Himed, "On the performance of the cross-correlation detector for passive radar applications," *Signal Processing*, vol. 113, pp. 32–37, 2015.

[7] F. Colone, P. Falcone, A. Macera, and P. Lombardo, "Two-dimensional location of moving targets within local areas using WiFi-based multistatic passive radar," *IET Radar, Sonar & Navigation*, vol. 8, no. 2, pp. 123–131, 2014.

[8] L. Wanchun, T. Qiu, H. Chengfeng, and L. Yingxiang, "Location algorithms for moving target in non-coherent distributed multiple-input multiple-output radar systems," *IET Signal Processing*, vol. 11, no. 5, pp. 503–514, 2017.

[9] L. Yang, L. Yang, and K. C. Ho, "Moving target localization in multistatic sonar using time delays, Doppler shifts and arrival angles," in *Proceedings of the IEEE International Conference on Acoustics, Speech and Signal Processing (ICASSP)*, pp. 3399–3403, New Orleans, LA, USA, March 2017.

[10] Y. Wei, W. Li, Q. Tang, P. Wei, and H. Zhang, "A closed-form location algorithm without auxiliary variables for moving target in noncoherent multiple-input and multiple-output radar system," *IEEE Access*, vol. 8, Article ID 69496, 69508 pages, 2020.

[11] P. E. Howland, D. Maksimiuk, and G. Reitsma, "FM radio based bistatic radar," *IEE Proceedings-Radar, Sonar and Navigation*, vol. 152, no. 3, pp. 107–115, 2005.

[12] J. Wang, H. Wang, and Y. Zhao, "Direction finding in frequency-modulated-based passive bistatic radar with a four-

element Adcock antenna array," *IET Radar, Sonar & Navigation*, vol. 5, no. 8, pp. 807–813, 2011.

[13] Z. Gao, R. Tao, and T. Shan, "Two fast algorithms of cross-ambiguity function for passive radar[J]," *Acta Electronica Sinica*, vol. 37, no. 3, pp. 669–672, 2009.

[14] Z. Zhuo, T. Shan, and R. Tao, "Fast computation of cross-ambiguity function[J]," *Journal of Beijing Institute of Technology (Social Sciences Edition)*, vol. 17, no. 4, pp. 466–471, 2008.

[15] J. Pidanic and Z. Nemec, "Speed-up the computing of bistatic cross-ambiguity function," in *Proceedings of the 13th International Radar Symposium*, pp. 310–313, Warsaw, Poland, May 2012.

[16] J. Zheng, R. Chen, T. Yang et al., "An efficient strategy for accurate detection and localization of UAV swarms," *IEEE Internet of Things Journal*, vol. 8, no. 20, 15381 pages, Article ID 15372, 2021.

[17] J. Zheng, T. Yang, H. Liu, T. Su, and L. Wan, "Accurate detection and localization of unmanned aerial vehicle swarms-enabled mobile edge computing system," *IEEE Transactions on Industrial Informatics*, vol. 17, no. 7, pp. 5059–5067, 2021.